Time-like observables: differential cross section and angular asymmetry

Dominique Marchand, Thierry Hennino, Ronald Kunne, Saro Ong, Béatrice Ramstein, Malgorzata Sudol, Egle Tomasi-Gustafsson

Time-like observables: differential cross section and angular asymmetry

D. Marchand, T. Hennino, R. Kunne, S. Ong,
B. Ramstein, M. Sudoł and E. Tomasi-Gustafsson*
Institut de Physique Nucléaire d'Orsay, CNRS/IN2P3,
and Université Paris Sud, 91406 Orsay, France

Abstract

Time-like electromagnetic form factors can be obtained from unpolarized measurements of the differential cross section in proton antiproton annihilation in a pair of leptons, as $\overline{p} + p \leftrightarrow e^+ + e^-$, with the $\overline{\mathrm{P}}$ANDA detector at FAIR. We study the sensitivity of such measurements and focus on observables such as the angular asymmetry and the ratio of electric to magnetic form factors. We also collect useful formulas and references for future simulations and studies.

* *IRFU/SPhN, CEA Saclay, 91191 Gif-sur-Yvette Cedex, France*

I. INTRODUCTION

In the time-like (TL) region the measurement of the differential cross section for the process $\overline{p}+p \to e^+ + e^-$ at a fixed value of the total energy squared s and for two different angles θ (angle between the electron and the antiproton momenta in the center of mass system -CMS), allows the separation of the two proton electromagnetic form factors (FFs), $|G_M|$ and $|G_E|$. This method corresponds to the well known Rosenbluth separation for the elastic ep-scattering. However in TL region, this procedure is simpler, as it requires to change only one kinematical variable, $\cos\theta$, whereas, in SL it is necessary to change simultaneously two kinematical variables: the energy of the initial electron and the electron scattering angle, fixing the momentum transfer squared, q^2.

The differential cross section for $\overline{p}+p \leftrightarrow e^+ + e^-$ can be expressed as a function of the nucleon TL electromagnetic FFs according to the following formula (which holds in CMS frame) [1]:

$$\frac{d\sigma}{d(\cos\theta)} = \frac{\pi\alpha^2}{8M^2\tau\sqrt{\tau(\tau-1)}}\left[\tau|G_M|^2(1+\cos^2\theta)+|G_E|^2\sin^2\theta\right],\ \tau=\frac{q^2}{4M^2}=\frac{s}{4M^2} \quad (1)$$

where θ is the angle between the electron and the antiproton in CMS, M is the proton mass, $\alpha = e^2/(4\pi) = 1/137$.

The angular dependence of the cross section, Eq. (1), results directly from the assumption of one-photon exchange, where the spin of the photon is equal to 1 and the electromagnetic hadron interaction satisfies the $C-$invariance. Therefore the measurement of the differential cross section at three angles (or more) would also allow to test the presence of two-photon exchange. From first principles, as the C-invariance of the electromagnetic interaction and the crossing symmetry, the presence of two-photon exchange creates a forward backward asymmetry in the time-like differential cross section. The analysis of the available data from [2] shows no asymmetry, within an error of 2% [3]. Such a value is of the order of the asymmetry expected from radiative corrections as calculated from QED [4]. It is expected that the relative role of the two-photon mechanism increases at relatively large momentum transfer in SL and in TL regions, for the same physical reasons, which are related to the steep decrease of the hadronic electromagnetic FFs, as previously discussed in [5] and more recently in [6, 7].

The individual determination of $|G_E|$ and $|G_M|$ in the TL region, has not been realized

yet. In order to have information on these FFs, due to the poor statistics, it is necessary to integrate the differential cross section over a wide angular range. One assumes that the G_E-contribution plays a minor role in the cross section at large q^2 and the experimental results are usually given in terms of $|G_M|$, under the hypothesis that $G_E = 0$ or $|G_E| = |G_M|$. The first hypothesis is arbitrary whereas the second one is strictly valid at threshold only, and there is no theoretical argument which justifies its validity at any other momentum transfer, where $q^2 \neq 4M^2$. Note, however, that the values of $|G_M|$ extracted under these two contradicting hypothesis differ at most by 20%. The relation $|G_E| = 3|G_M|$ has also been considered in connection with dispersion relation studies, which allow to extrapolate from the TL region to the SL region [8]. The values of G_M in the TL region, obtained under the assumption that $|G_E| = |G_M|$, are larger than the corresponding SL values. This has been considered as a proof of the non applicability of the Phràgmen-Lindelöf theorem, or as an evidence that the asymptotic regime is not reached [9].The Phragmèn-Lindelöf theorem constrains definitely FFs in TL and in SL regions to have the same value at large q^2. Assuming its validity, from Eq. (1) we can deduce $|G_E|$, using the existing experimental data from the $\overline{p} + p \leftrightarrow e^+ + e^-$ reaction [10]. On the other hand, taking for $|G_E|$ the SL values, affects very little the values of G_M, due to the kinematical factor τ, which weights the magnetic contribution to the differential cross section and makes the contribution of the electric FF to the cross section very small.

With the antiproton beam which will be available at FAIR[1], the $\overline{\mathrm{P}}$ANDA experiment will be able to measure precise angular distributions up to large values of q^2 [11]. The purpose of this note is to investigate how electromagnetic FFs could be extracted at best from such experiment, based on extrapolation of the available cross section data and with the present hypothesis on the available luminosity at $\overline{\mathrm{P}}$ANDA . The plan of this note is the following:

- Different parametrizations of TL magnetic FF (dipole-like, QCD-inspired..) are compared and different assumptions for G_E: $G_E = 0$, $G_E = G_M$, $G_E = 3G_M$ are considered (Section II).

- Angular distributions are built, assuming the total cross section known, for different values of q^2 in the range 5.4-27 GeV^2 (Section III).

[1] Facility for Antiproton and Ion Research (Darmstadt, Germany)

- We define a variable, the angular asymmetry, which depends only on q^2, and which enhances the difference of the angular dependence of the electric ($\sin^2\theta$) and magnetic ($1+\cos^2\theta$) factors (see Eq. 1) with respect to the value of the differential cross section at 90° (Section IV).

- The angular distributions are fitted by two-parameter functions, where the parameters are a normalization constant and the form factor ratio $\mathcal{R} = |G_E|/|G_M|$ or $\mathcal{R}^2$, or the angular asymmetry and the cross section at $\theta = \pi/2$ (Section V).

- The relative errors on these two quantities, FF ratio and angular asymmetry are illustrated and discussed (Section VI).

- A summary and a few comments will be given in Conclusions. The Appendix collects different spectra, which may be useful for further studies.

II. PARAMETRIZATIONS OF TL FFS

The form factors, in particular $|G_M|$, depend in principle only on the four momentum squared of the virtual photon, q^2, which corresponds to the total energy s where the measurement is performed. The cross section is usually integrated over a limited angular range.

Attempts of determining the ratio $\mathcal{R} = |G_E|/|G_M|$ can be found in Refs. [12] (LEAR) and more recently in Ref. [2] through the reaction $e^+ + e^- \to \overline{p} + p + \gamma$ (BABAR Collaboration), corrected by the initial state radiation. The results, although affected by large errors, are not in agreement, giving, in the second case a value for the ratio larger than unity, in a wide q^2 range above threshold.

A. Note on the space-like region

In the space-like (SL) region the situation is different. The cross section for the elastic scattering of electrons on protons is sufficiently large to allow the measurements of the angular distribution and/or of polarization observables. The existing data on G_M show a dipole behavior up to the highest measured value, $-q^2 \simeq 31$ GeV^2, according to

$$G_M(q^2)/\mu_p = G_d, \text{ with } G_d = \frac{1}{\left(1 - \dfrac{q^2}{m_d^2}\right)^2}, \; m_d^2 = 0.71 \text{ GeV}^2. \tag{2}$$

It should be noticed that, in the SL region, the independent determination of both G_M and G_E FFs, from the unpolarized $(e^- p)$-cross section, has been done up to $-q^2 = 8.7$ GeV^2 [13]. Further extraction of G_M [14] assumes $G_E = G_M/\mu_p$. The behavior of G_E, deduced from polarization experiment $p(\vec{e}, e')\vec{p}$ differs from G_M/μ_p, with a deviation from G_d up to 75% at $-q^2$=5.8 GeV^2 [15]. This is the maximum momentum at which the new precise data are available in SL region. It corresponds to values of q^2 above threshold of the reaction $\overline{p} + p \rightarrow e^+ + e^-$, when translated to TL region. The results of an extension of this measurement up to $-q^2$=9 GeV^2 will be available.

B. Time-like region: models for $|G_M|$

Different parametrizations reproduce the magnetic form factor $|G_M|$ in the TL region, and are built as analytical extensions of models which reproduce the SL data, or inspired by asymptotic q^2 dependence as prescribed by QCD:

1. The behavior of $|G_M^{(TL)}|$ can be described by a modified dipole-like form such as :

$$|G_M^{(TL)}| = \frac{22.5}{\left(1 + \frac{q^2}{m_{nd}^2}\right)} \times G_d \tag{3}$$

where $m_{nd}^2 = 3.6$ GeV^2 has been fitted to the existing data in [10] and G_d is a function of q^2 as defined for the SL region (see Eq. 2).

Going to the TL region, the calculation of G_d can be based on an analytical extension (usual consideration) or on symmetry considerations with respect to the $q^2 = 0$ axis.

Under analytical extension q_{SL}^2 is replaced by $q_{TL}^2 = -q_{SL}^2$ in Eq. (2) which leads to the following formula for G_d^A (-A- standing for analytical), in TL region:

$$|G_d^{(TL)\,A}| = \frac{1}{\left(1 + \frac{q^2}{m_d^2}\right)^2} = \frac{1}{\left(1 + \frac{s}{m_d^2}\right)^2} \tag{4}$$

Under the symmetry considerations, we consider the absolute value of q_{TL}^2 which implies the same value of G_d in TL and SL regions for the same value of $|q^2|$. Therefore the expression for G_d, as defined in the SL region, Eq. (2), remains unchanged (-S-

standing for symmetric):

$$|G_d^{(TL)\,S}| = \frac{1}{\left(1 - \dfrac{q^2}{m_d^2}\right)^2} = \frac{1}{\left(1 - \dfrac{s}{m_d^2}\right)^2} \tag{5}$$

From Figs. 1 and 2, it can be seen that $G_d^{(TL)\,S}$ deviates from $G_d^{(TL)\,A}$ at low q^2 (46% at q^2=5 GeV^2) but as $q^2 \to \infty$ both parametrizations of $G_d^{(TL)}$ tend to the same zero limit.

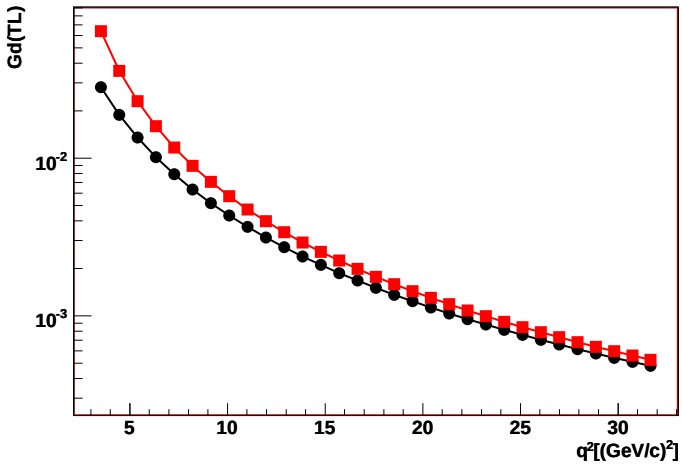

FIG. 1: $G_d^{(TL)}$ versus q^2 using the analytical extension (circles) and the symmetric form (squares).

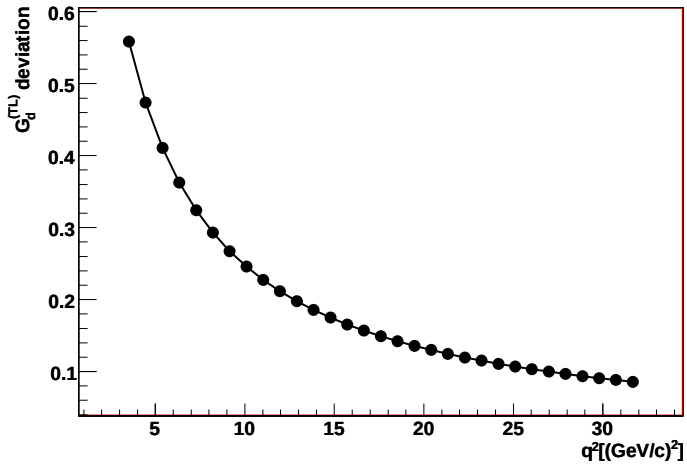

FIG. 2: Deviation between the two dipole-like form factors $G_d^{(TL)\,S}$ and $G_d^{(TL)\,A}$ shown in Fig. 1.

2. A commonly used parametrization of the data on the magnetic form factor of the proton in the TL region [16] is suggested by asymptotic QCD:

$$|G_M^{(TL)\,QCD}| = \frac{C}{s^2 \log^2(s/\Lambda^2)} \sim \frac{\alpha_s^2}{s^2} \tag{6}$$

where α_s is the strong coupling constant, $\Lambda = 0.3$ GeV, and $C = 56.3$ GeV^4 is a fitting parameter [17]. However, this form gives unphysical divergences for α_s, at small s ($s \ll \Lambda^2$).

3. Corrections based on dispersion relations have been suggested in [18] to avoid 'ghost' poles in α_s, and can be included in the following form:

$$|G_M^{(TL)\,QCDbis}| = \frac{\mathcal{D}}{s^2 \left[\log^2(s/\Lambda^2) + \pi^2\right]}. \tag{7}$$

where $\mathcal{D} = 89.45$ GeV^4.

The behavior of the different parametrizations is shown in Fig. 3. These parametrizations reproduce the annihilation data up to ~ 12 GeV^2, at least and differ by 20% at $q^2 = 15$ GeV^2.

III. ANGULAR DISTRIBUTIONS

Angular distributions can be calculated from Eq. (1) according to different parametrizations for G_M and three different possible relations between G_E and G_M. In Table I, let us give an order of magnitude of the expected number of events.

Let us assume the total cross section known. Then, according to the different relations among G_E and G_M, one can build the differential cross section. If the total cross section (integral) is fixed, the three curves in Figs. 4 and 5 correspond to different assumptions on G_E. In particular it is visible for collinear kinematics, where the electric contribution vanishes.

According to the different parametrizations, for six q^2 values in the range $5.4 \leq 27$ GeV^2, angular distributions are built. The number of counts is integrated in $\cos\theta$ bin of width equal to 0.2 and shown in the following figures: Fig. 4 corresponds to parametrization (4), Fig. 5 corresponds to parametrization (7). Two more plots corresponding to Eqs. (5) and (6), given for comparison, are shown in the Appendix, Figs. 26 and 27.

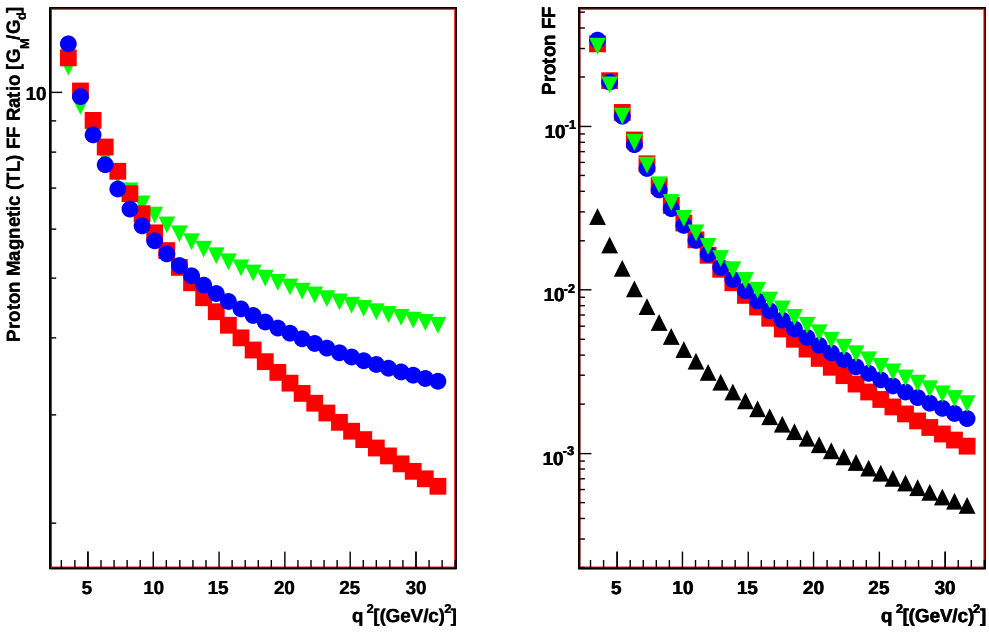

FIG. 3: Comparison of different G_M parametrizations (right), including the dipole form (black triangles): from Eq. (3) (red squares), from Eq. (7) (green triangle down), from Eq. (6) (blue circles). Same, but scaled by dipole (left).

The reported error is the statistical error calculated from the expected counting rate assuming a data taking period of 10^7 s and a luminosity $2{\cdot}10^{32}$ cm^{-2}/s with 100% acceptance and efficiency.

IV. ANGULAR ASYMMETRY

Let us introduce a quantity, the angular asymmetry, A, which enhances the different angular behavior of the electric and magnetic terms with respect to $\theta = 90^0$. The angular behavior is illustrated in Fig. 6. The electric term is accompanied by a dependence in $\sin^2\theta$. It means that, whatever is the value of $|G_E|^2$, it has a maximum at $\cos\theta = 0$ and vanishes at $\cos\theta = \pm 1$. So, the largest contribution of the G_E term to the cross section is at $\theta = 90°$. The magnetic term has a maximum at $\cos\theta = \pm 1$, which equals $2\tau|G_M|^2$ and a minimum

q^2[GeV^2]	τ	E_{kin}[GeV]	$p_{\bar{p}}$[GeV/c]	$\sigma_{tot}^{G_M^A}$[pb]	$N_{tot}^{G_M^A}$	$N^{G_M^A}$/day	$\sigma_{tot}^{G_M^{QCD\,bis}}$[pb]	$N_{tot}^{G_M^{QCD\,bis}}$	$N^{G_M^{QCD\,bis}}$/day
5.4	1.53	1.	1.7	538	1.1 10^6	9504	481.2	9.6 10^5	8295
8.2	2.33	2.5	3.3	32	6.4 10^4	553	32.7	6.5 10^4	562
12.9	3.66	5.	5.9	1.6	3.2 10^3	28	2.2	4.3 10^3	37
16.7	4.73	7.	7.9	0.29	580	5	0.49	979	8.5
17.6	5.00	7.5	8.4	0.20	400	3.5	0.36	713	6.1
22.3	6.33	10.	10.9	0.04	81	0.7	0.09	183	1.6
27.	7.66	12.5	13.4	0.01	22	0.2	0.03	62	0.5

TABLE I: Under the assumption $G_E = G_M$, expected counting rates corresponding to an integrated luminosity $\mathcal{L} = 2 \cdot 10^{39}$ cm^{-2} for $\overline{p} + p \to e^+ + e^-$ taking into account full acceptance and 100% efficiency.

at $\cos\theta = 0$, which equals $\tau |G_M|^2$.

One can express the angular dependence of the differential cross section as a function of the angular asymmetry $\mathcal{A}$ as:

$$\frac{d\sigma}{d(\cos\theta)} = \sigma_0 \left[1 + \mathcal{A}\cos^2\theta\right], \tag{8}$$

where σ_0 is the value of the differential cross section at $\theta = \pi/2$ and $\mathcal{A}$ can be written as a function of the FFs:

$$\mathcal{A} = \frac{\tau|G_M|^2 - |G_E|^2}{\tau|G_M|^2 + |G_E|^2} = \frac{\tau - \mathcal{R}^2}{\tau + \mathcal{R}^2},\ \mathcal{R} = \frac{|G_E|}{|G_M|}. \tag{9}$$

The angular asymmetry $\mathcal{A}$ lies in the range $-1 \leq \mathcal{A} \leq 1$. For $G_E = 0$ one obtains $\mathcal{A} = 1$ and for $G_E = G_M$ one obtains $\mathcal{A} = (\tau - 1)/(\tau + 1)$ (see Table II).

	$\mathcal{A}$	$\mathcal{R}$
$\lvert G_E\rvert = 0$	1	0
$\lvert G_E\rvert = \lvert G_M\rvert$	$(\tau - 1)/(\tau + 1)$	1
$\lvert G_E\rvert = 3\lvert G_M\rvert$	$(\tau - 9)/(\tau + 9)$	3

TABLE II: Values of $\mathcal{A}$ and $\mathcal{R}$ according to different assumptions for $|G_E|$.

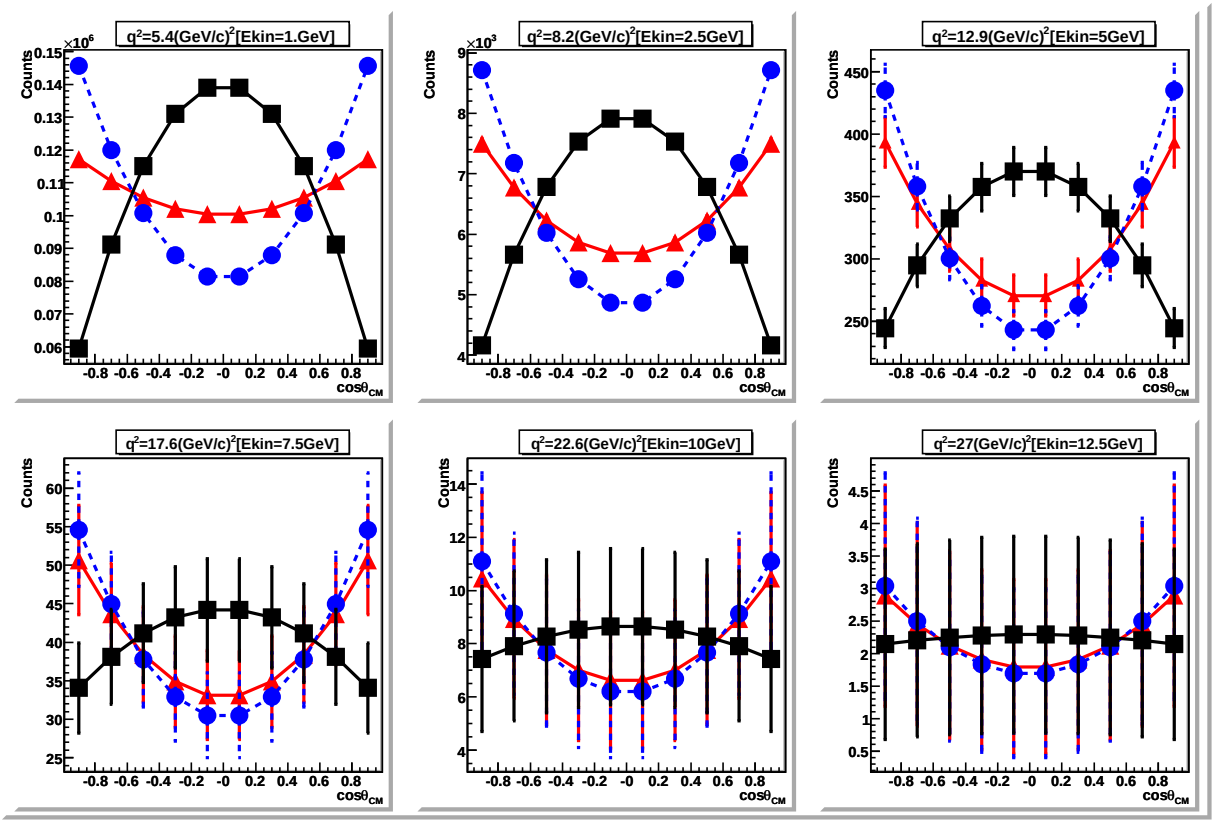

FIG. 4: Angular distribution as a function of $\cos\theta_{CM}$ in the hypothesis of G_E=0 (blue open symbols, dashed line), G_E=G_M (red solid symbols) and G_E=3G_M (black solid symbols), for q^2 values ranging from 5.4 to 27 GeV^2. The values for G_M are computed from Eq. (4).

In the limit of small errors, as long as first order statistical methods work, the error on $\mathcal{A}$ is obtained from the error on $\mathcal{R}$ deriving Eq. (9):

$$\Delta\mathcal{A} = \frac{4\mathcal{R}\tau}{(\tau+\mathcal{R}^2)^2}\Delta\mathcal{R} \tag{10}$$

and it is a function of τ. Let us illustrate this function:

- For $\tau \ll 1$: $\Delta\mathcal{A}$ behaves as $(4\tau/\mathcal{R}^3)\Delta\mathcal{R}$, and the normalization $\mathcal{R}(q^2=0) = 1/\mu_p$ (μ_p is the proton magnetic moment) is known, it is finite and positive, for proton.
- At threshold: $G_E = G_M$, $\tau = 1$, $\mathcal{A} = 0$, $\mathcal{R} = 1$, $\Delta\mathcal{A} = \Delta\mathcal{R}$.
- For $\tau \gg 1$: $\Delta\mathcal{A} \to 0$ as $(4\mathcal{R}/\tau)\Delta\mathcal{R}$. Note that, assuming QCD scaling laws [19], $\mathcal{R} \to$ constant.

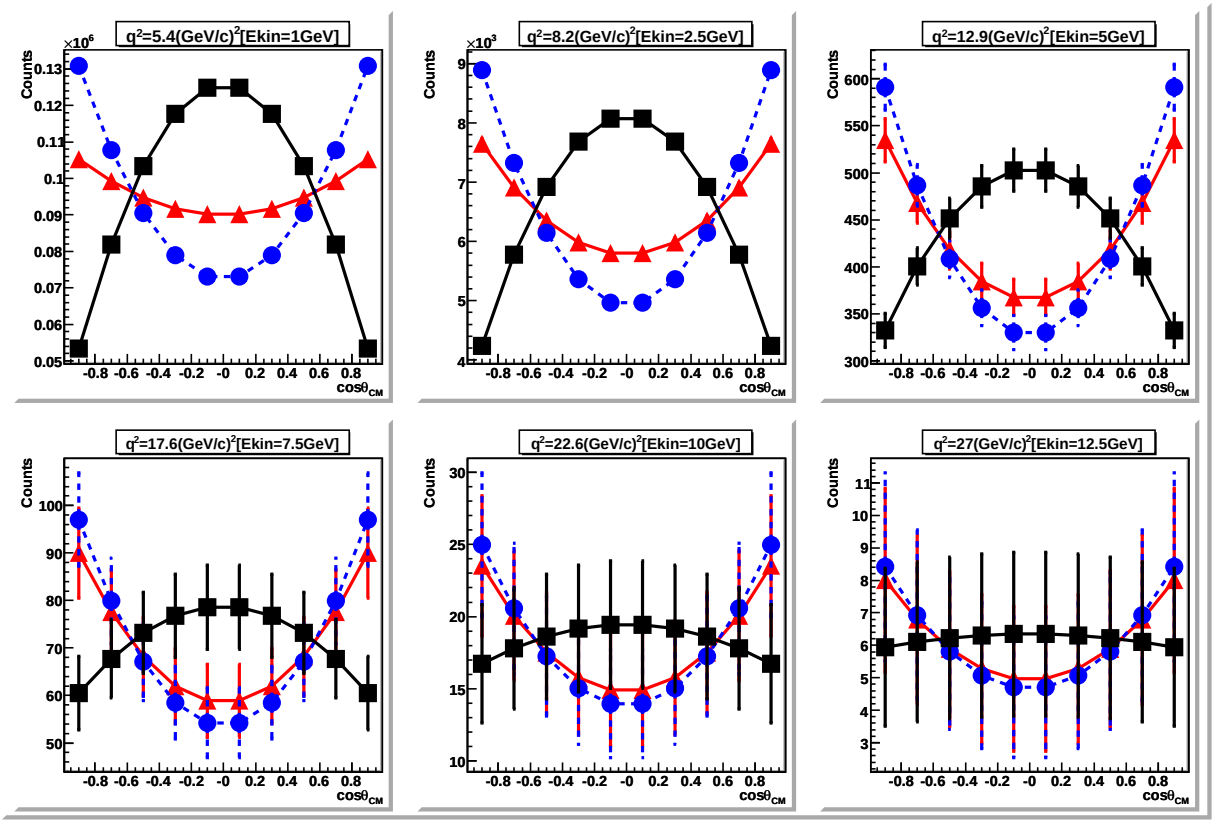

FIG. 5: Same as Fig. 26, for FFs parametrization corresponding to Eq. (7).

In Fig. 7 the dependence of $\Delta\mathcal{A}$ as a function of τ is shown, for constant $\mathcal{R}$, $\Delta\mathcal{R} = 1$. $\Delta\mathcal{A}$ is never larger than $\Delta\mathcal{R}$.

Integrating Eq. (1) over $\cos\theta$ from -1 to $+1$, one gets the total cross section σ_{tot}:

$$\sigma_{tot} = 2\sigma_0 \left(1 + \frac{\mathcal{A}}{3}\right) \tag{11}$$

Therefore, knowing the total cross section and the cross section σ_0 at $\theta = \pi/2$, one can express $\mathcal{A}$ as:

$$\mathcal{A} = \frac{3(\sigma_{tot} - 2\sigma_0)}{2\sigma_0} \tag{12}$$

with

$$\Delta\mathcal{A} = \frac{3}{2\sigma_0} \times \sqrt{(\Delta\sigma_{tot})^2 + \left(\frac{\sigma_{tot}}{\sigma_0}\right)^2 \times (\Delta\sigma_0)^2} \tag{13}$$

Knowing the total cross section and the value of the cross section at $\pi/2$ with their associated experimental errors, one can use Eqs. (12) and (13) to compute the angular asymmetry $\mathcal{A}$ corresponding to different hypothesis on the electric FF. Fig. 8 shows this asymmetry as

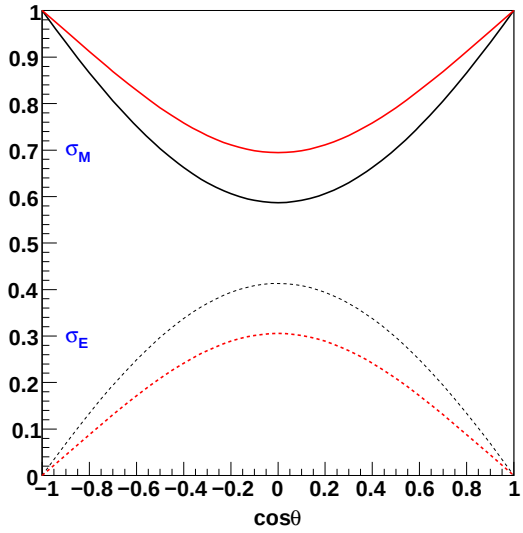

FIG. 6: Relative contribution of the electric σ_E (dashed lines) and magnetic σ_M (solid lines) terms to the differential cross section for $\bar{p} + p \rightarrow e^+ + e^-$, as functions of $\cos\theta$ for two different values of q^2: 5 GeV^2 (red lines) and q^2 =8 GeV^2 (black lines).

a function of q^2 for G_E=0, G_E=G_M and G_E=3G_M. For this figure the value of the cross section at $\pi/2$ corresponds to the number of counts integrated in the $\cos\theta$ range $[-0.1, 0.1]$.

Note that in real experiments, the angular range where the measurement can be performed is usually restricted to $|\cos\theta| \leq \bar{c}$ with $\bar{c} = \cos\theta_{max} \sim 0.7$. One can still define the angular asymmetry in the same way, replacing σ_{tot} by :

$$\sigma_{int} = 2\sigma_0\,\bar{c}\left(1 + \frac{\mathcal{A}}{3}\,\bar{c}^2\right) \tag{14}$$

Within 'ideal' conditions (full acceptance, 100% efficiency, ...), from Fig. 8, one can see that the hypothesis G_E=0 and G_E=G_M can be discriminated up to $q^2 \sim 9$ GeV^2. Nevertheless we will see in the next section that extracting $\mathcal{A}$ from the angular distributions leads to small errors and allows to separate these two hypothesis up to higher q^2.

V. FITTING THE DIFFERENTIAL CROSS SECTION

In real experiments or in simulations, one builds differential cross section as a function of $\cos\theta$, and then one can extract FFs from a fitting procedure, using MINUIT. We will limit the angular range to $|\cos\theta| \leq 0.8$, to be closer to realistic experimental conditions.

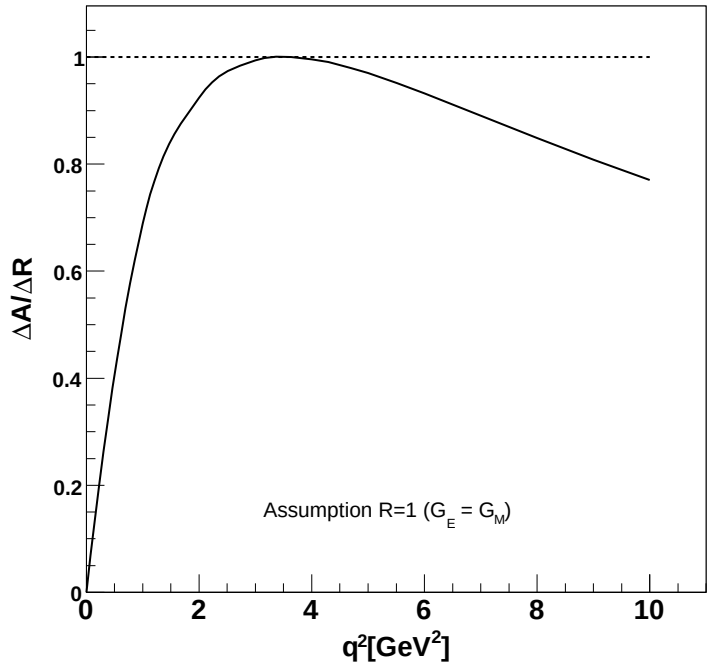

FIG. 7: Error on the angular asymmetry, assuming a constant error on the FFs ratio $\mathcal{R}$.

Knowing the absolute normalization (luminosity, efficiency, acceptance..), it is possible to determine separately: $|G_E|^2$, $|G_M|^2$. One can determine the ratio of FFs, instead of G_E and G_M separately, and a global normalization factor, if the absolute cross section is not precisely known. One can also do a two parameter fit, determining, instead, the angular asymmetry and the cross section at 90°.

Let us first introduce the measured number of events in a given 0.2 wide bin interval centered at $\cos\theta$: $N(\cos\theta)$. It is related to the cross section by a proportionality constant, which contains not only the kinematical factor $\mathcal{N}_0$, but also the integrated luminosity of the measurement $\mathcal{L}$ as well as efficiency ϵ and acceptance A (which are considered equal to unity, as a first step).

A two parameter fit of the distributions corresponding to Fig. 5, has been done, using two functions. The first function allows to extract the asymmetry $\mathcal{A}$:

$$N(\cos\theta) = p_{10}(1 + p_{11}\cos^2\theta) \tag{15}$$

and the second one, as in our case the normalization is known, allows a direct extraction of

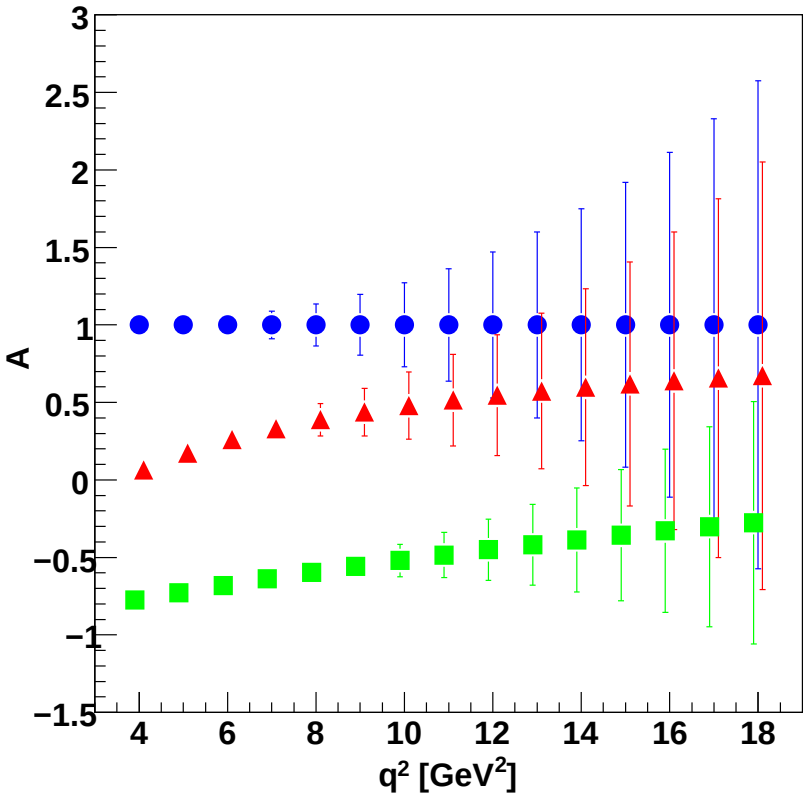

FIG. 8: Angular asymmetry from Eq. (12) as a function of q^2 for $G_E = 0$ (circles), $G_E = G_M$ (triangles) and $G_E = 3G_M$ (squares). The values for G_M are computed from Eq. (4).

$|G_E|^2$, $|G_M|^2$:

$$N(\cos\theta) = \epsilon A \mathcal{L} \mathcal{N}_0 [\tau\, p_{20}^2 (1 + \cos^2\theta) + p_{21}^2\, \sin^2\theta],\ \mathcal{N}_0 = \frac{\hbar^2 c^2 \pi \alpha^2}{8M^2\sqrt{\tau(\tau-1)}}. \qquad (16)$$

Eq. (16) gives results from the ratio $\mathcal{R}$, which are equivalent to another possible two-parameter fit:

$$N(\cos\theta) = p_{30}[\tau\,(1 + \cos^2\theta) + p_{31}^2\, \sin^2\theta], \qquad (17)$$

The parameters $p_{10} \equiv N_0$, (N_0 is the number of counts at 90^0, $p_{11} \equiv \mathcal{A}$, $p_{20} \equiv G_M$, $p_{21} \equiv G_E$, and $p_{31} \equiv \mathcal{R}$ are determined by a least squared fit on the data, for each distribution, at each value of q^2. Their values are related by Eq. (9).

To show the relative error in the extraction with the different type of fits, the results for the ratio (open circles) and the asymmetry (solid circles) are reported in Fig. 9 as a function of q^2, for the case $G_E = 0$ where $\mathcal{R}$=0 and $\mathcal{A} = 1$. For the case $G_E = G_M$ the

results are shown in Fig. 10, where $\mathcal{R}$=1 and $\mathcal{A} = (\tau - 1)/(\tau + 1)$, and in Fig. 11 for the case $G_E = 3G_M$, where $\mathcal{R}$=3, and $\mathcal{A} = (\tau - 9)/(\tau + 9)$. When $G_E = 0$, the determination of $\mathcal{R}$ becomes very imprecise, as the convergence with MINUIT strongly depends on the initial conditions. As the derivatives with respect to $\mathcal{R}$ diverge, one has to deal with instabilities in the minimization procedure. A more stable solution can be found considering $\mathcal{R}^2$ instead of $\mathcal{R}$ as minimization parameter. But in such case, the convergence is obtained by allowing this parameter varying in negative interval, too.

The same results are plotted in Fig. 12 for the ratio and in Fig. 13 for the asymmetry, in order to have a direct comparison of the sensitivity of the same quantity for the considered hypothesis on FFs. The results for the error when $\mathcal{R} = 0$ are not meaningful, for the reasons given above. This issue will be discussed further. The overlap of the projected errors for $\mathcal{A}$ will occur for $q^2 \geq 15$ GeV^2.

The relative precision on the errors of these three quantities can be appreciated from Fig. 14, where the relative error $\Delta\mathcal{A}/\Delta\mathcal{R}$ is given as a function of q^2. One can see that the $\Delta\mathcal{A}/\Delta\mathcal{R}$ ratio is always smaller than unity in all the considered range of q^2. The relative error on the asymmetry is shown in Fig. 15, and on the ratio in Fig. 16. $\Delta\mathcal{A}$ increases, as expected, with q^2 but it is in general smaller than for $\mathcal{R}$.

Again, care must be taken during the fitting procedure. One can meet different kinds of instabilities: in particular for Eq. (16), in the case when $G_E = 0$, one constrains the procedure to fit with two parameters, whereas the cross section depends on one parameter (the term G_E becoming negligible, compared to the magnetic term). A minimization program, based on derivatives, can not converge easily. In this case it is more favorable to take the corresponding expression in $\mathcal{R}^2$ (17).

For the fits based on Eqs. (15,17) problems can arise from the fact that the two parameters are not really independent, and the correlation coefficients can be quite large. However, in this case, the relevant parameter, related to $\mathcal{A}$ corresponds to a modulation around a constant value, and it is more sensitive to the details of the distribution.

Once the quantities $\mathcal{R}$, $\mathcal{R}^2$ and $\mathcal{A}$ are extracted from the data, models which give predictions for G_E and G_M can be compared directly to the chosen observable, according to the most favorable conditions.

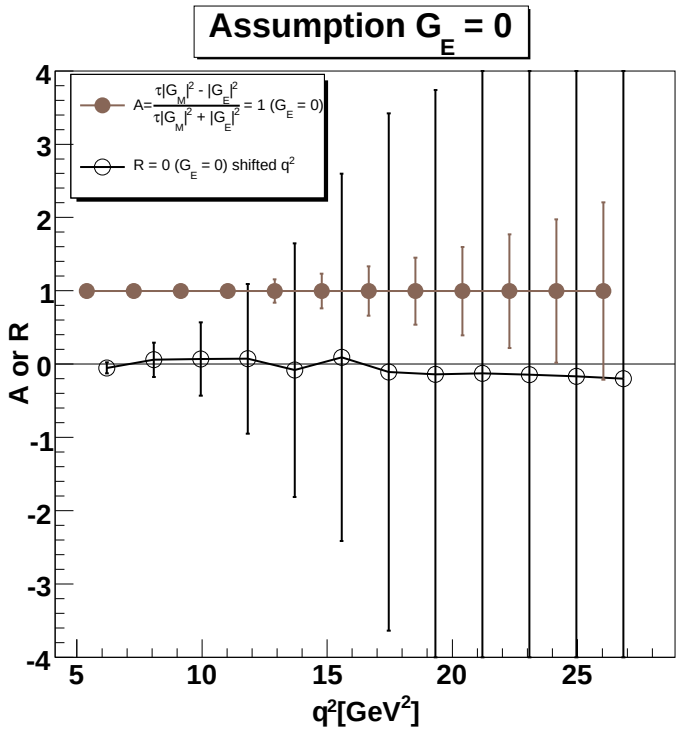

FIG. 9: Angular asymmetry (solid circles) and form factor ratio (open circles) from the corresponding fits of the angular distribution built for $G_E = 0$ and assuming G_M from Eq. (7). For clarity, the abscissa for $\mathcal{R}$ has been shifted by 0.8 GeV^2. Fits are from Eqs. (15,17).

VI. STUDY OF ERRORS

Fits have also been performed using MINUIT on spectra built on a large number of Monte Carlo events. Therefore the points are perfectly aligned on the distribution in $\cos^2\theta$: the χ^2 is very small and the parameter value are very near to the input parameters, without large fluctuations. We can do the following observations:

- For $\mathcal{R} = 0$:
  - The fit on $\mathcal{R}$ is unreliable, unstable as shown in Figs. 9 and 12.
  - One can do a MINUIT fit on $\mathcal{R}^2$ allowing negative range for the minimization.
  - The fit on $\mathcal{A}$ is reliable, stable up to $q^2 = 16.7$ GeV^2, at least.
- The distribution of $\mathcal{R}^2$ derived statistically from a set of histograms is not symmetric at 16.7 GeV^2, which means that the mean and the maximum value do not coincide. In

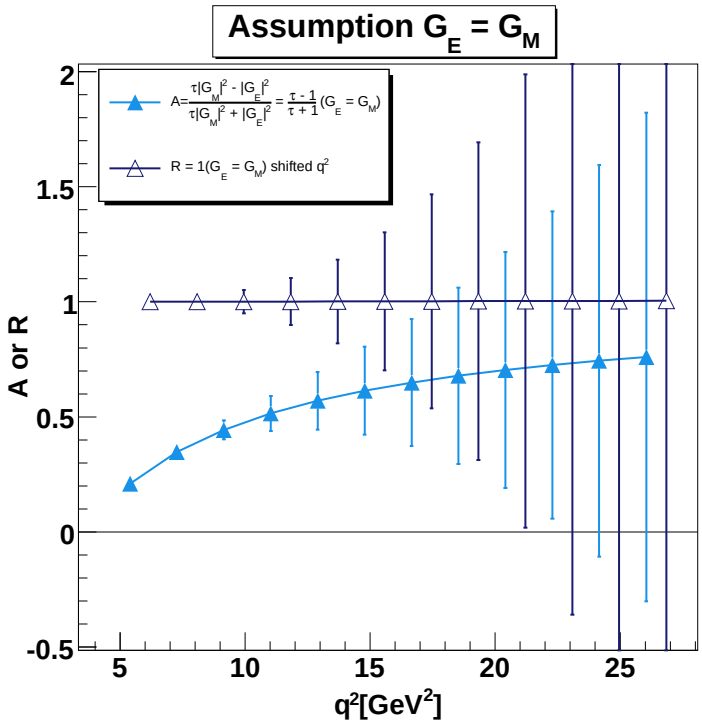

FIG. 10: Same as in Fig. 9, but for $G_E = G_M$.

this case, one should take asymmetric errors if one defines the error as 66% probability of finding the value inside the range.

- Negative $\mathcal{R}^2$ give a problem for deriving $\mathcal{R}$, as well as values of $\mathcal{A}$ outside the interval: $-1 \leq \mathcal{A} \leq 1$.

Let us collect the following formulas which relate $\mathcal{R}$, $\mathcal{R}^2$, and $\mathcal{A}$:

$$\mathcal{A} = \frac{\tau - \mathcal{R}^2}{\tau + \mathcal{R}^2} \tag{18}$$

$$\mathcal{R}^2 = \frac{\tau(1 - \mathcal{A})}{\mathcal{A} + 1} \tag{19}$$

$$\mathcal{R} = \sqrt{\frac{\tau(1 - \mathcal{A})}{\mathcal{A} + 1}} \tag{20}$$

It is possible to calculate in different ways the ratio R and its error.

- (1) We fit the angular distributions with Eq. (17). The fit has two parameters, p_{30} and $p_{31} = \mathcal{R}$. This method should be taken with care for $\mathcal{R} = 0$, as the minimization is unstable.

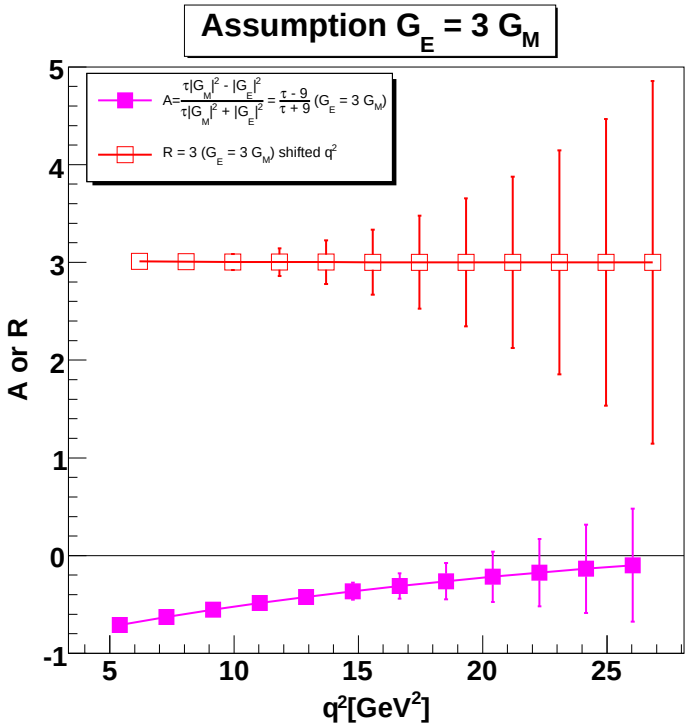

FIG. 11: Same as in Fig. 9, but for $G_E = 3G_M$.

- (2) $\mathcal{R}^2$-interval: we derive $\mathcal{R}$ from $\mathcal{R}^2$, found from a fit of the angular distributions with the formula (21) and we calculate the interval $\Delta\mathcal{R}^2 = \{\mathcal{R}^2_{max} - \mathcal{R}^2_{min}\}$. The fit gives a symmetric interval around $\mathcal{R}^2$. If we translate this interval into $\mathcal{R}$, the interval around $\mathcal{R}$ is not symmetric. Moreover, for $\mathcal{R}^2 = 0$ the lower limit is negative (and even $\mathcal{R}^2$ extracted from the fit can be negative).

- (3) $\mathcal{R}^2$-analytic : We derive $\mathcal{R}$ from $\mathcal{R}^2$, found from a fit of the angular distributions with a two parameter (p_{30} and $\beta \equiv \mathcal{R}^2 \equiv p^2_{31}$) formula:

$$N(\theta) = p_{30}[\beta(\sin^2\theta) + \tau(1 + \cos^2\theta)], \tag{21}$$

  and then we calculate $\Delta\mathcal{R} = \Delta\mathcal{R}^2/2/\mathcal{R}$. This method does not work for $\mathcal{R} = 0$ and does not work at large q^2 where the error on $\mathcal{R}^2$ is large and the distribution over $\mathcal{R}^2$ not gaussian.

- We do a two parameter fit ($\alpha = \sigma_0$ and $\beta = \sigma_0\mathcal{A}$) of the angular distribution using the angular asymmetry with respect to $\theta = 90°$:

$$N(\theta) = \alpha + \beta\cos^2\theta. \tag{22}$$

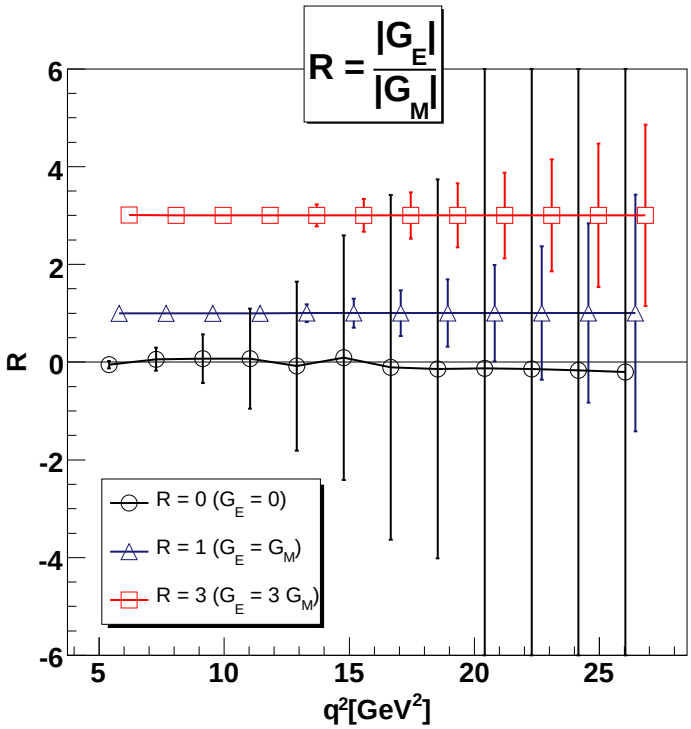

FIG. 12: Form factor ratio for $G_E = 0$ (circles), $G_E = G_M$ (triangles), $G_E = 3G_M$ (squares). For clarity the abscissa are shifted by 0.4 (0.8) GeV^2 for $G_E = G_M$ ($G_E = 3G_M$). The values for G_M are computed from Eq. (7). Fits are from Eqs. (15,17).

The fit is very stable, for all the three considered cases ($\mathcal{R}$=0, $\mathcal{R}$=1 and $\mathcal{R}$=3) and the distribution of $\mathcal{A}$ is symmetric all along q^2. We calculate the error on $\mathcal{R}$ from $\mathcal{A}$:

- (4) $\mathcal{A}$-interval: the fit is done on $\mathcal{A}$, then we use the interval $\Delta\mathcal{A} = \{\mathcal{A}_{max} - \mathcal{A}_{min}\}$ and find the correspondence $\{\mathcal{R}_{max} - \mathcal{R}_{min}\}$. This works when $\mathcal{A} \pm \Delta\mathcal{A}$ is in the kinematically allowed interval [-1;+1], which is not the case, for example, when $G_E = 0$ ($\mathcal{A} = 1$) .
- (5) $\mathcal{A}$-analytic: by derivation of (20)

$$\Delta\mathcal{R} = \frac{\tau}{\mathcal{R}} \frac{\Delta\mathcal{A}}{(\mathcal{A}+1)^2} \tag{23}$$

This underestimate the error, if the error on $\mathcal{A}$ is very large.

- (6) Monte-Carlo simulation approach: one generates N times a random angular distribution, with a given total number of events $N_{ev}(q^2)$, which includes the statistical fluctuations within each 0.2 wide $\cos\theta$ bin. For each set of $N_{ev}(q^2)$, out of the N

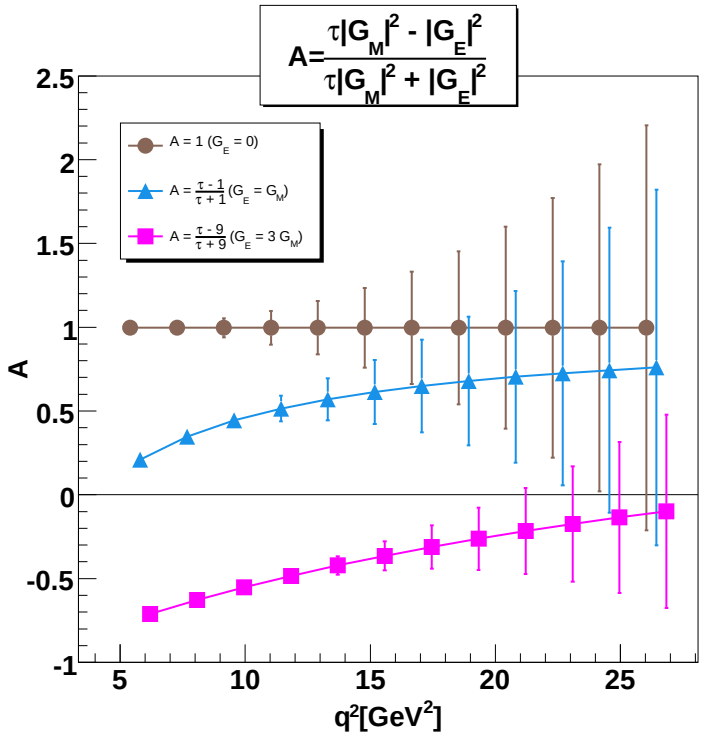

FIG. 13: Same as in Fig. 12 but for the angular asymmetry.

samples, one fits the angular distribution, obtaining a well defined value of the ratio $\mathcal{R}^2$. The histogram of the distribution from the N simulations, gives then access to the errors on $\mathcal{R}^2$, from which the distribution on $\mathcal{R}$ and $\mathcal{A}$ can be directly obtained. If such distributions are gaussian, one can extract the width in terms of σ, or confidence levels with associated confidence intervals. This is especially helpful for the case $\mathcal{R} = 0$ for which no negative value has to be considered. Note that the distributions used for the confidence intervals are not gaussian-like for $q^2 \geq 13.8$ GeV^2 even for $\mathcal{R} \neq 0$.

The results are summarized in table III. $\mathcal{R}$ with the errors derived in the different cases is shown in the Figs. 17, 18, and 19, respectively for $\mathcal{R}$=0, $\mathcal{R}$=1 and $\mathcal{R}$=3, with the following convention: the point in black, in the middle is the value from the fit, at the left side, the values from $\mathcal{R}^2$ are shown, and, at the right side from $\mathcal{A}$ and from Monte Carlo. For $\mathcal{R} = 0$, the analytic derivation with symmetric error is reported, as well as the Monte Carlo solution. In Table IV the confidence interval and the corresponding confidence level are given for different q^2, in the case $\mathcal{R} = 0$.

- black: case 1 error derived from the fit (Minuit),

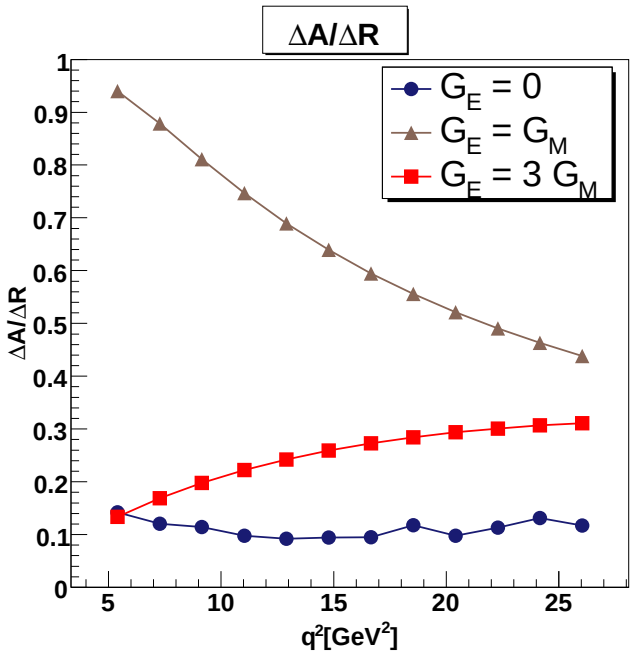

FIG. 14: $\Delta\mathcal{A}/\Delta\mathcal{R}$ as a function of q^2 corresponding to $G_E = 0$ (circles), $G_E = G_M$ (triangles) and $G_E = 3G_M$ (squares). $\Delta\mathcal{A}$ being the error on the angular asymmetry and $\Delta\mathcal{R}$ the error on the FF ratio. The values for G_M are computed from Eq. (7). Fits are from Eqs. (15,17).

- red: case 2 from $\mathcal{R}^2$, interval - asymmetric at large q^2,
- green: case 3 from $\mathcal{R}^2$, analytic, symmetric,
- blue: case 4 from $\mathcal{A}$, interval - asymmetric at large q^2,
- cyan: case 5 from $\mathcal{A}$, analytic, symmetric.
- magenta: case 6 from Monte Carlo.

One can see that, for $q^2 \leq 11$ GeV^2, the errors obtained with the different methods are in agreement within 10% as long as they are small ($\leq 30\%$). In this case, the first order calculation of errors is sufficient and the distributions with the Monte Carlo method are symmetric.

The lines in Figs. 17, 18, and 19, correspond to models as in [17]: two component VMD (solid line, green), VMD/QCD (dash-dotted, blue); QCD-like (dashed,red).

For $\mathcal{R}^2$: in the case $\mathcal{R}$=0, only the errors from the fit are reported. For $\mathcal{R}$=1 and $\mathcal{R}$=3

- black: case 1 error derived from the fit (MINUIT)

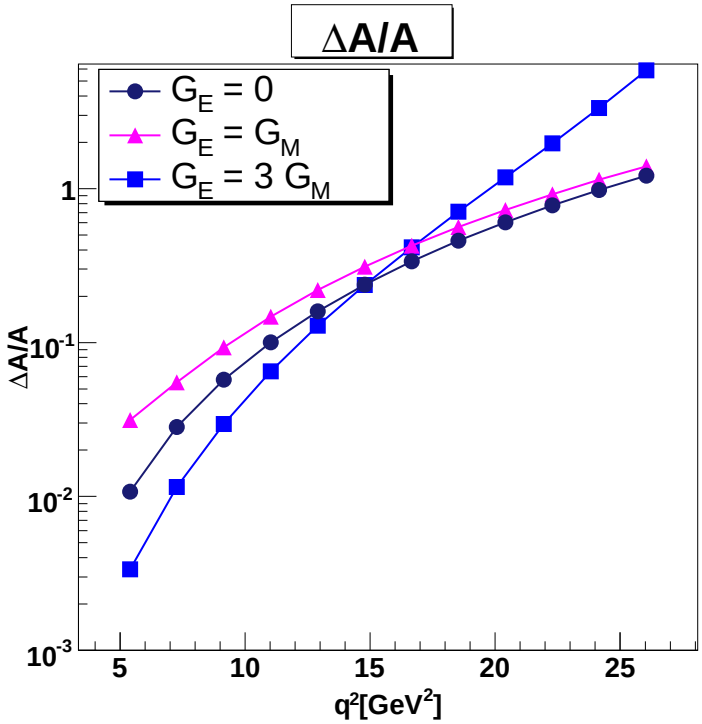

FIG. 15: Relative error on the angular asymmetry $\mathcal{A}$ corresponding to $G_E = 0$ (circles), $G_E = G_M$ (triangles) and $G_E = 3G_M$ (squares). The values for G_M are computed from Eq. (7). Fits are from Eqs. (15,17).

- blue: case 4 from $\mathcal{A}$, interval, asymmetric
- cyan: case 5 from $\mathcal{A}$, analytic, symmetric

In Fig. 22 the behavior of $\mathcal{R}$ (solid line), Eq. (20) and $\mathcal{R}^2$ (dashed line), Eq. (19), as a function of $\mathcal{A}$ is reported for two different q^2 values: 5.4 GeV^2 (red lines) and 16.4 GeV^2 (black lines).

It appears from Fig. 22 that a symmetric interval around a value of $\mathcal{A}$ will translate into an asymmetric interval on $\mathcal{R}$ or $\mathcal{R}^2$. It appears also that the ordinate is very much dilated compared to the abscissa. This effects become more dramatic as q^2 increases.

Questions on the extraction of $\mathcal{R}$ arise when $\mathcal{R} = 0$, when the error is large, and when the range is not symmetric. The final suggestion is to report the data as in Figs. 21, 23, and 24. In these cases, the errors are symmetric and well under control.

At large q^2, when the individual determination of FFs is affected by too large errors, one can still extract a generalized form factor (F_p) from the integrated cross section, in the

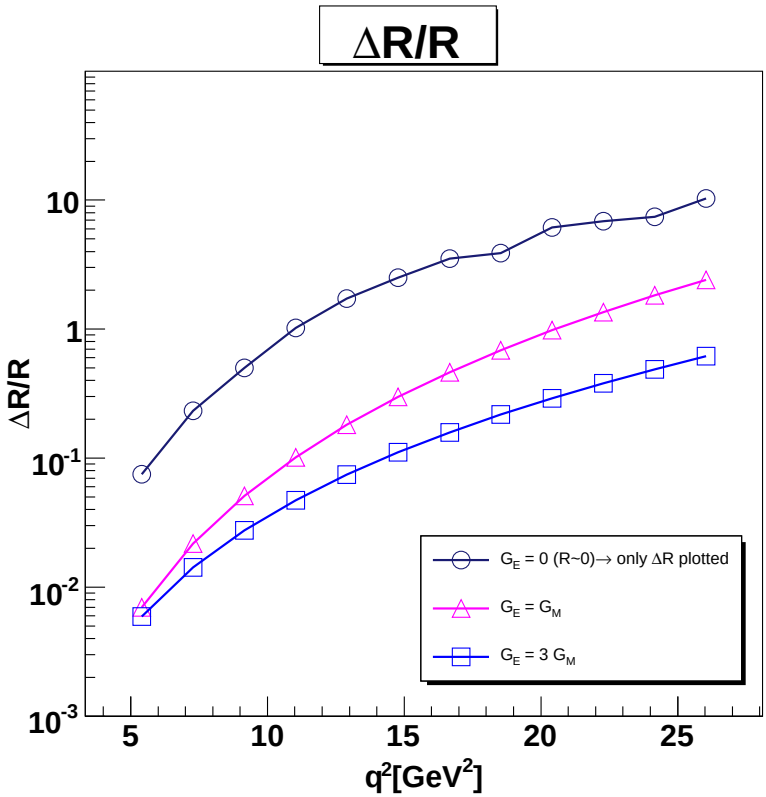

FIG. 16: Relative error on $\mathcal{R}$ corresponding to $G_E = 0$ (circles), $G_E = G_M$ (triangles) and $G_E = 3G_M$ (squares). Note that for $G_E = 0$ only $\Delta\mathcal{R}$ is plotted as $\mathcal{R} = 0$. The values for G_M are computed from Eq. (7).

hypothesis $\mathcal{R}$=0, or $\mathcal{R}$=1. This is shown, for $\mathcal{R}$=1 in Fig. 25, and it is equivalent to a measurement of cross section. The errors reported here take into account a global efficiency and acceptance, extrapolated from realistic Monte Carlo simulations (as well as a reduced angular range $|\cos\theta| \leq 0.8$).

VII. GENERALIZED TIME-LIKE PROTON FORM FACTOR

The experimental situation for the generalized proton form factor, F_p, which can be extracted from the time-like total cross section, in the hypothesis $|G_E| = |G_M|$ is shown together with the world data (Fig. 25). The last point, for q^2=27 GeV^2, corresponds to 22 events for the standard conditions of integrated luminosity $\mathcal{L} = 2\cdot 10^{39}$ cm^{-2} and parametrization Eq. (4). Assuming identification and reconstruction efficiency equal to 0.04, by extrapolation from Monte Carlo estimates, one event will be measured. Let us give

the notations and the corresponding references for the different experiments:

Notations

- red full circles Babar [2]
- green open lozenge E835 [20, 21]
- blue open circles Fenice [22]
- gray open stars PS170 [23]
- blue asterisk E760 [24]
- black squares : expected $\overline{\mathrm{P}}$ANDA : the errors are from simulation (full squares) or extrapolation from simulation (open squares).
- green full triangles DM1 [25]
- green open squares DM2 [26]
- cyan open cross BES [27]
- blue triangle down CLEO [28]

VIII. CONCLUSIONS

We have studied the angular dependence of the differential cross section for the annihilation reaction $\bar{p} + p \rightarrow e^+ + e^-$, in the framework of one photon exchange, and its sensitivity to different choices of the electromagnetic FFs, G_E and G_M.

We have expressed the differential cross section which contains the proton electromagnetic TL FFs, $|G_E|$ and $|G_M|$ as a function of the ratio $\mathcal{R} = |G_E|/|G_M|$ (which appears as squared). We have defined the angular asymmetry $\mathcal{A}$ as a deviation of the distribution from the cross section at 90°, wich is basically the slope of the linear dependence of the cross section as a function of $\cos^2\theta$.

Let us note that the relations analyzed here, between G_E and G_M i.e., $\mathcal{R}$ =0 or 1 are those commonly taken for the data analysis. One expects $G_E = G_M$ near threshold, therefore $\mathcal{R}$ =1 seems to be probable for τ around 1. $\mathcal{R} = 3$, which corresponds to negative values of

$\mathcal{A}$, has been also considered, as it was predicted by theoretical models as VMD or dispersion relations for $q^2 \geq 10$ GeV^2.

Up to $q^2 = 11$ GeV^2, all the fit methods (excepted the case $\mathcal{R} = 0$) give similar results for the errors on the observables. From 12 GeV^2 on, the Monte Carlo method clearly shows that non linearities appear and that confidence intervals are no longer symmetric. The error derived from a MINUIT Gaussian fit for $\mathcal{R}$ and $\mathcal{R}^2$ becomes more and more problematic as q^2 increases. The advantage of the Monte Carlo is that it is valid everywhere since it contains by itself all the correlations and the error propagation to all orders. In particular for the case $\mathcal{R} = 0$, confidence intervals corresponding to confidence levels have been given.

The ratio $\mathcal{R}$ can be extracted up to 12-14 GeV^2 with an error comparable to the one obtained by BaBar at much lower q^2. At low q^2 values, the quality of the determination of the ratio is typically better by an order of magnitude compared to the existing data.

A temptative comparison with predictions from models which reproduce the SL region and are analytically extrapolated to the TL region [17], show that up to 14 GeV^2 at least, one will discriminate from a VMD model and QCD extrapolated predictions. The asymmetry $\mathcal{A}$ (extracted as the slope of the differential cross section as a function of $\cos^2\theta$) can be also directly compared to models.

From the integrated cross section, one can still extract a generalized form factor, at even larger q^2 values, assuming $G_E = 0$ or $G_E = G_M$. At 28 GeV^2 one expects, for $G_E = G_M$ one count in four months data taking, with nominal luminosity, assuming average efficiency of 0.04 and following parametrization (4).

Let us stress that the results presented here hold for one photon exchange. As a matter of fact, the angular dependence of the cross section, Eq. (1), results directly from the assumption of one-photon exchange, where the spin of the photon is equal 1 and the electromagnetic hadron interaction satisfies the $C-$invariance. The possible presence of two photon exchange would induce a different odd $\cos\theta$ terms in the angular distribution, and an expected enhancement of the cross section at large q^2. This issue will be discussed in a separate report.

IX. ACKNOWLEDGMENTS

Thanks are due to J. van de Wiele for interesting discussions and to J. Boucher for a careful reading.

---

[1] A. Zichichi, S. M. Berman, N. Cabibbo, R. Gatto, Nuovo Cim. **24**, 170 (1962).

[2] B. Aubert *et al.* [BABAR Collaboration], Phys. Rev. D **73**, 012005 (2006).

[3] E. Tomasi-Gustafsson, E. A. Kuraev, S. Bakmaev and S. Pacetti, Phys. Lett. B **659**, 197 (2008);

[4] E. A. Kuraev, A. I. Ahmadov, S. N. Panov and E. Tomasi-Gustafsson, Nucl. Phys. A **816**, 89 (2009).

[5] J. Gunion and L. Stodolsky, Phys. Rev. Lett. **30**, 345 (1973); V. Franco, Phys. Rev. D **8**, 826 (1973); V. N. Boitsov, L.A. Kondratyuk and V.B. Kopeliovich, Sov. J. Nucl. Phys **16**, 287 (1973); F. M. Lev, Sov. J. Nucl. Phys. **21**, 45 (1973).

[6] M. P. Rekalo, E. Tomasi-Gustafsson and D. Prout, Phys. Rev. **C60**, 042202R (1999).

[7] G. I. Gakh and E. Tomasi-Gustafsson, Nucl. Phys. A **771**, 169 (2006).

[8] S. Pacetti, Eur. Phys. J. A **32**, 421 (2007).

[9] S. M. Bilenky, C. Giunti, V. Wataghin, Z. Phys. **C59**, 475 (1993).

[10] E. Tomasi-Gustafsson and M. P. Rekalo, Phys. Lett. B **504** (2001) 291.

[11] E. Tomasi-Gustafsson and M. P. Rekalo, Int. Report DAPNIA 04-01, arXiv:0810.4245 [hep-ph].

[12] G. Bardin *et al.*, Nucl. Phys. **B411**, 3 (1994).

[13] L. Andivahis *et al.*, Phys. Rev. D **50**, 5491 (1994).

[14] R. G. Arnold *et al.*, Phys. Rev. Lett. **57**, 174 (1986).

[15] M. K. Jones *et al.*, Phys. Rev. Lett. 84 (2000) 1398; O. Gayou *et al.*, Phys. Rev. Lett. 88 (2002) 092301; V. Punjabi *et al.*, Phys. Rev. C 71 (2005) 055202 [Erratum-ibid. C **71** (2005) 069902].

[16] M. Andreotti *et al.*, Phys. Lett. B **559**, 20 (2003) and refs herein.

[17] E. Tomasi-Gustafsson, F. Lacroix, C. Duterte and G. I. Gakh, Eur. Phys. J. A 24 (2005) 419.

[18] D. V. Shirkov and I. L. Solovtsov, Phys. Rev. Lett. **79**, 1209 (1997); arXiv:hep-ph/0611229.

[19] V. A. Matveev, R. M. Muradian, and A. N. Tavkhelidze, Lett. Nuovo Cim. 7, 719 (1973); S. J. Brodsky and G. R. Farrar, Phys. Rev. Lett. 31, 1153 (1973).

[20] M. Ambrogiani *et al.* [E835 Collaboration], Phys. Rev. D **60**, 032002 (1999);

[21] M. Andreotti *et al.*, Phys. Lett. B **559**, 20 (2003).

[22] A. Antonelli *et al.*, Nucl. Phys. B **517**, 3 (1998).

[23] G. Bardin *et al.*, Nucl. Phys. B **411**,3 (1994).

[24] T. A. Armstrong *et al.* [E760 Collaboration], Phys. Rev. Lett. **70**, 1212 (1993).

[25] B. Delcourt *et al.*, Phys. Lett. B **86**, 395 (1979).

[26] D. Bisello *et al.*, Nucl. Phys. B **224**, 379 (1983).

[27] M. Ablikim *et al.* [BES Collaboration], Phys. Lett. B **630**, 14 (2005).

[28] T. K. Pedlar *et al.* [CLEO Collaboration], Phys. Rev. Lett. **95**, 261803 (2005).

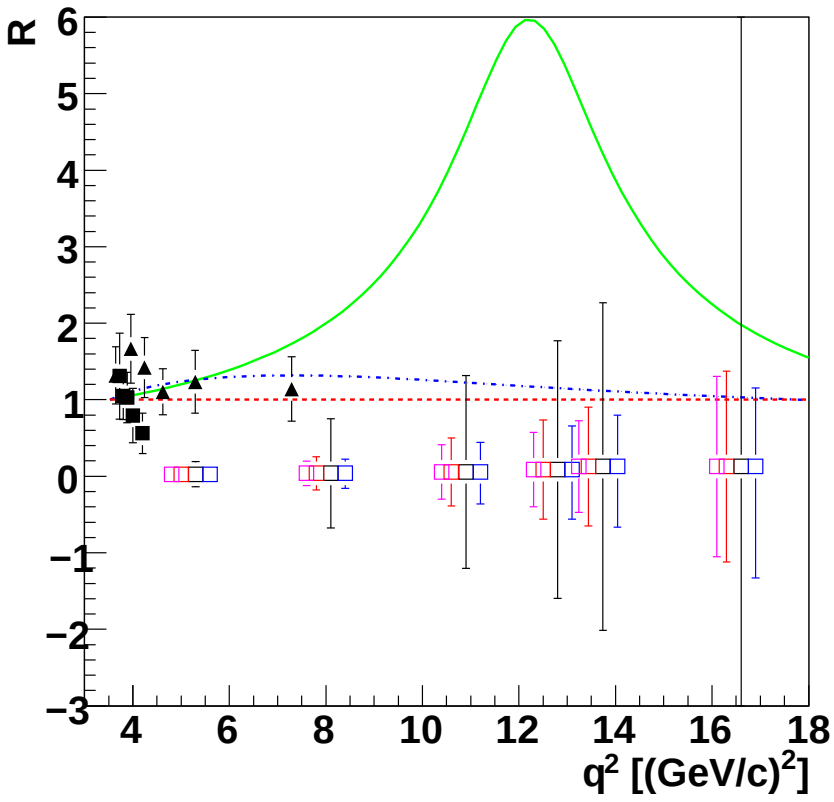

FIG. 17: $\mathcal{R}$ as a function of q^2, for $G_E = 0$, and the different calculations. For each q^2 the point corresponding to the fit is in black; at the left: from MC (magenta), $\mathcal{R}^2$-interval (red); at the right: A-interval (blue). Models: two component VMD (green solid line), VMD/QCD Lomon, (blue dash-dotted line); QCD-like (red dashed line). (see text).

q^2 (GeV^2)	R	$\Delta\mathcal{R}(1)$	$\{\Delta\mathcal{R}\}(2)$	$\Delta\mathcal{R}(3)$	$\{\Delta\mathcal{R}\}(4)$	$\Delta\mathcal{R}(5)$	$\Delta\mathcal{R}(6)$
5.4	0	< 0.076	< 0.165	-	<0.069	-	-
	1	$^{+0.009}_{-0.009}$	0.009	0.009	$^{+0.009}_{-0.009}$	0.009	0.009
	3	$^{+0.029}_{-0.029}$	0.026	0.029	$^{+0.038}_{-0.038}$	0.037	0.031
8.2	0	<0.215	<0.714	-	<0.197	-	-
	1	$^{+0.046}_{-0.048}$	0.047	0.047	$^{+0.044}_{-0.044}$	0.044	0.048
	3	$^{-0.108}_{+0.109}$	0.107	0.107	$^{+0.126}_{-0.115}$	0.120	0.102
11	0	< 0.443	< 1.259	-	< 0.419	-	-
	1	$^{+0.149}_{-0.176}$	0.161	0.161	$^{+0.149}_{-0.148}$	0.148	0.188
	3	$^{+0.256}_{-0.280}$	0.282	0.267	$^{+0.340}_{-0.278}$	0.305	0.308
12.9	0	<0.650	<1.681	-	< 0.646	-	-
	1	$^{+0.284}_{-0.409}$	0.325	0.325	$^{+0.313}_{-0.298}$	0.298	0.324
	3	$^{+0.438}_{0.514}$	0.501	0.469	$^{+0.641}_{-0.459}$	0.530	$^{+0.62}_{-0.42}$
13.84	0	< 0.777	<2.14	-	< 0.789	-	-
	1	$^{+0.378}_{-0.680}$	0.449	0.449	$^{+0.458}_{-0.411}$	0.412	$^{+0.54}_{-0.51}$
	3	$^{+0.741}_{-0.591}$	0.654	0.649	$^{+0.878}_{-0.576}$	0.686	$^{+0.90}_{-0.53}$
16.70	0	<1.247	<8.098	-	< 1.454	-	-
	1	$^{+0.788}_{-1.002}$	1.105	1.098	$^{+1.001}_{-1.036}$	1.014	< 1.69
	3	$^{+1.152}_{-2.124}$	1.398	1.373	$^{+2.649}_{-1.072}$	1.430	$^{+3}_{-2.13}$

TABLE III: Error on $\mathcal{R}$, for different q^2 values, and for the 6 cases (see text), taking into account efficiency and acceptance.

q^2[GeV^2]	CL = 68%	80%	90%	95%
5.4	0.072	0.094	0.115	0.129
8.2	0.157	0.217	0.273	0.312
11.0	0.355	0.481	0.604	0.693
12.9	0.485	0.663	0.849	0.980
13.84	0.600	0.822	1.05	1.23
16.7	1.18	1.68	2.33	3.03

TABLE IV: Confidence levels and confidence intervals for the case $\mathcal{R}$=0, corresponding to different values of q^2.

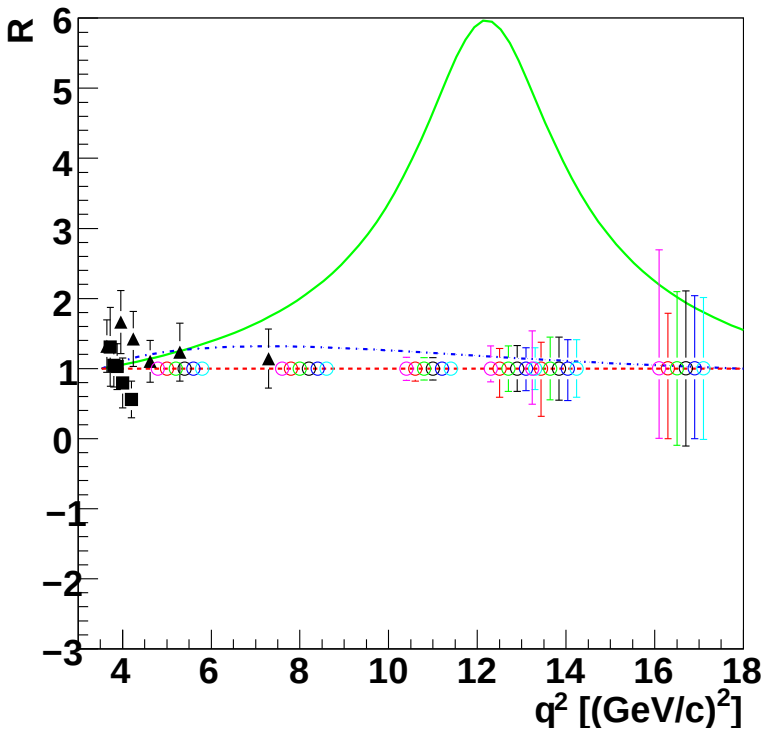

FIG. 18: $\mathcal{R}$ as a function of q^2, for $G_E = G_M$, and the different calculations. For each q^2 the point corresponding to the fit is in black; at the left: from MC (magenta), $\mathcal{R}^2$-interval (red); $\mathcal{R}^2$-analytic (green); at the right: $\mathcal{A}$-interval (blue); $\mathcal{A}$-analytic (cyan) (see text).

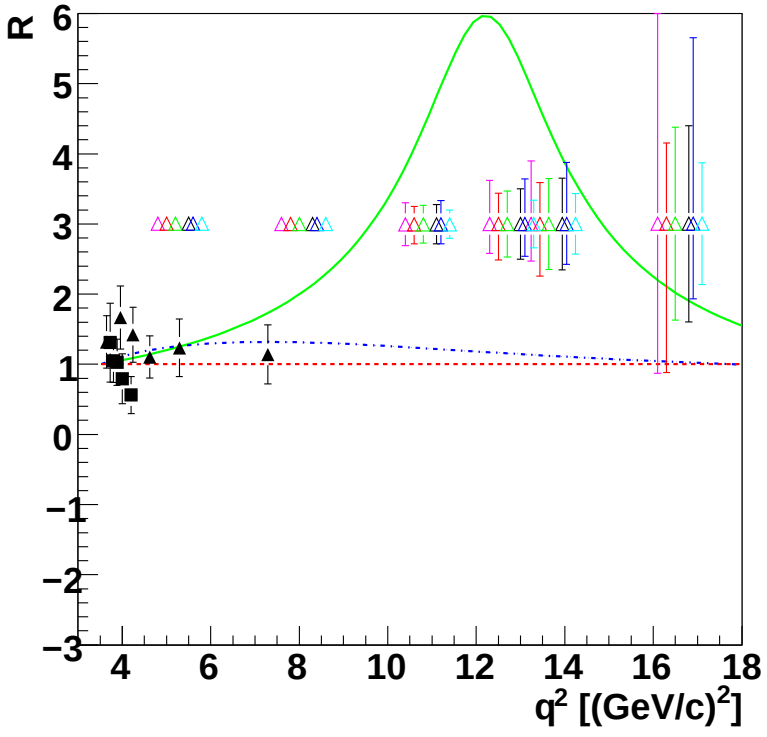

FIG. 19: $\mathcal{R}$ as a function of q^2, for $G_E = 3G_M$, and the different calculations (see text).

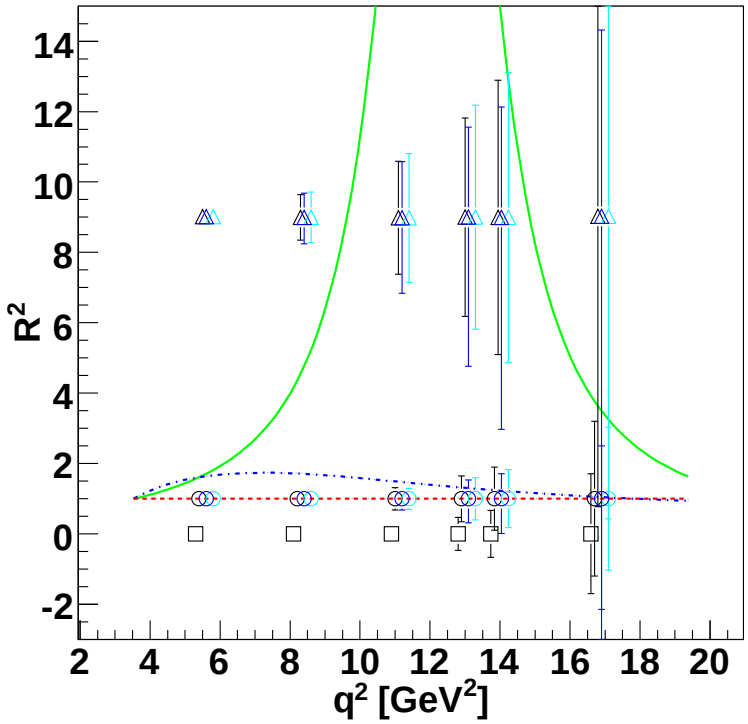

FIG. 20: $\mathcal{R}^2$ as a function of q^2, for $G_E = 0$ (squares), $G_E = G_M$ (circles) and $G_E = 3G_M$ (triangles).

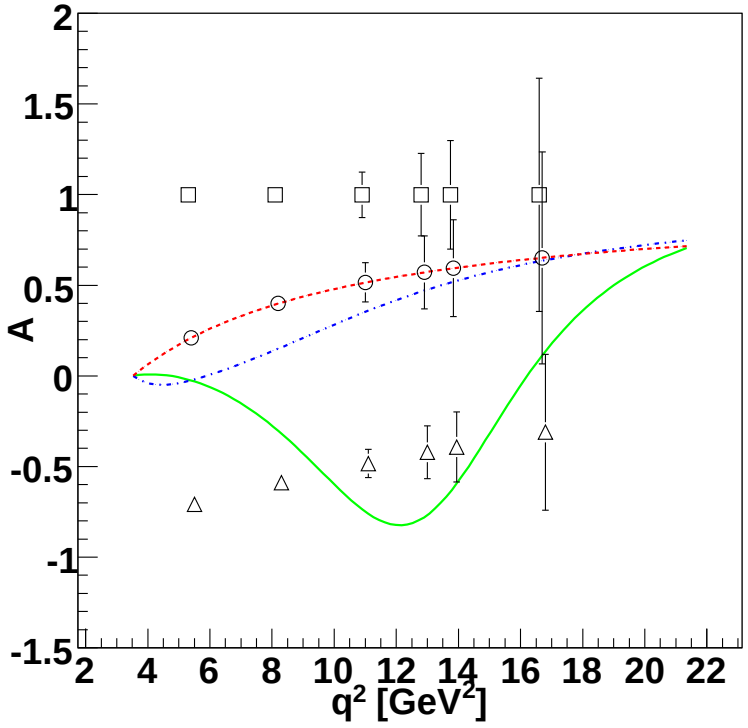

FIG. 21: $\mathcal{A}$ as a function of q^2, for $G_E = 0$ (squares), $G_E = G_M$ (circles) and $G_E = 3G_M$ (triangles). The reported errors correspond to the MINUIT fit according to Eq. (22).

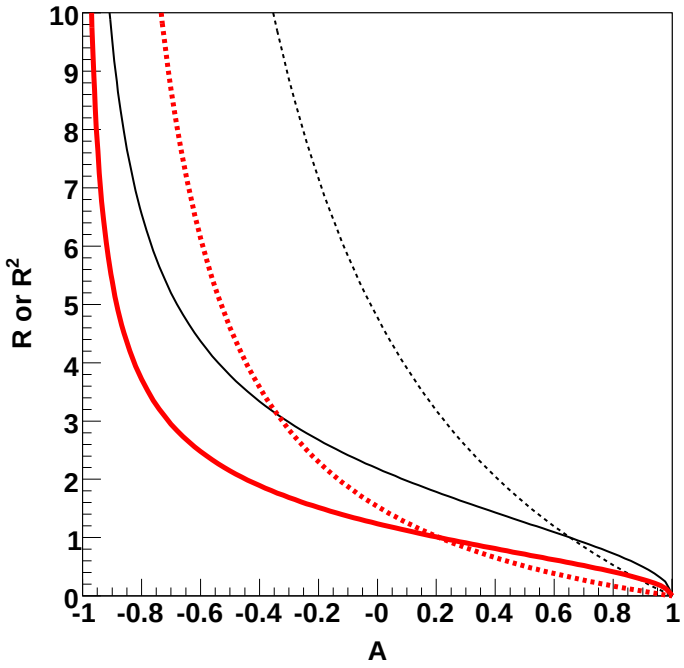

FIG. 22: $\mathcal{R}$ (solid line) and $\mathcal{R}^2$ (dashed line) as a function of $\mathcal{A}$ at $q^2 = 16.4$ GeV^2 (black lines) and 5.4 GeV^2 (red lines).

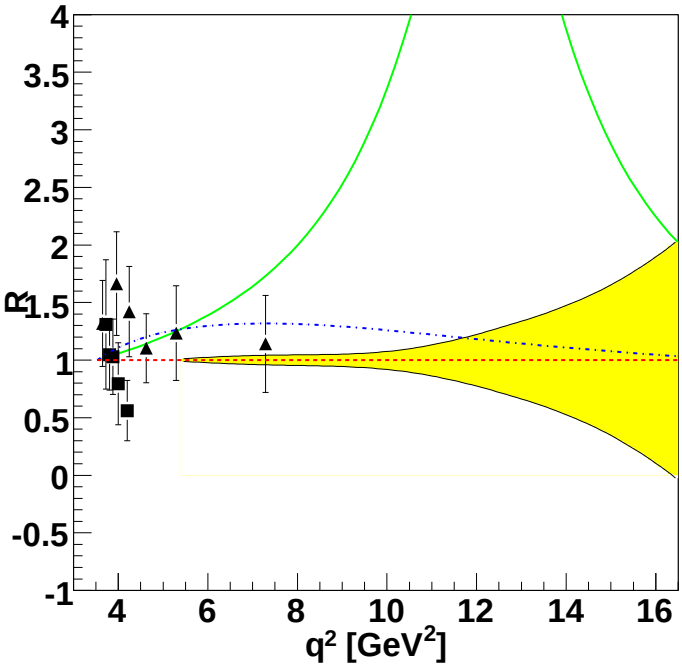

FIG. 23: $\mathcal{R}$ as a function of q^2, for $G_E = G_M$, and the different calculations (see text).

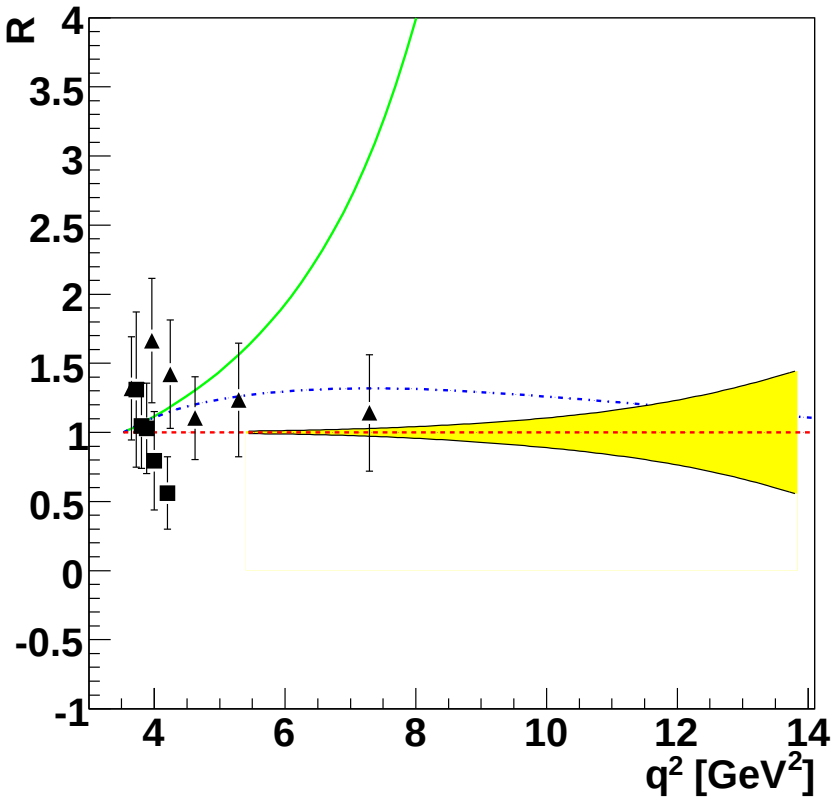

FIG. 24: Same as Fig. 24, reduced abscissa.

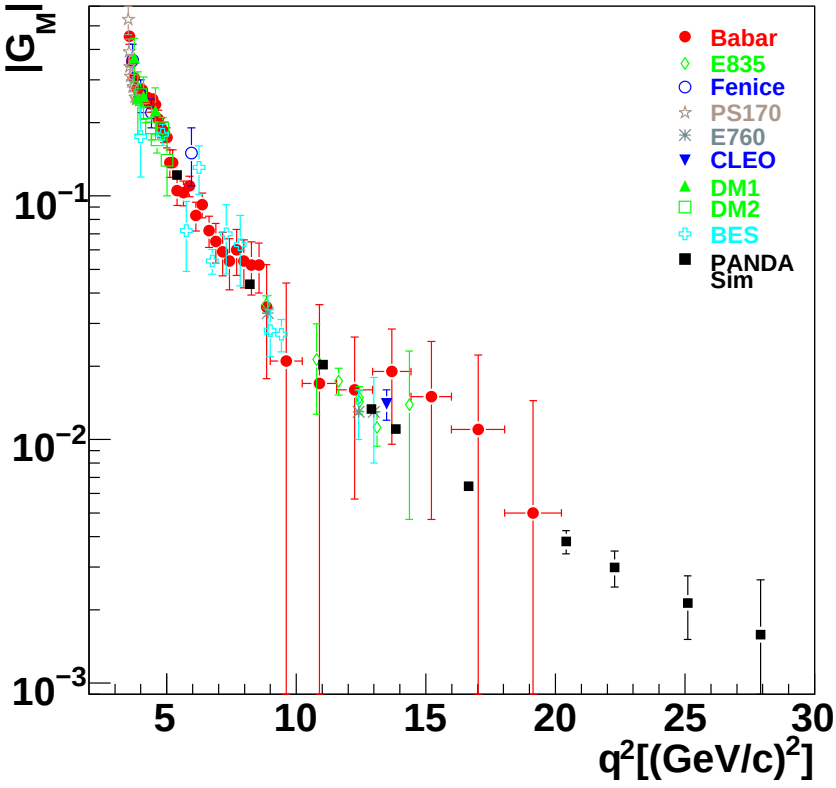

FIG. 25: Generalized proton form factor, from the annihilation cross section, in the hypothesis $G_E = G_M$.

X. APPENDIX : EXAMPLES OF ANGULAR DISTRIBUTIONS

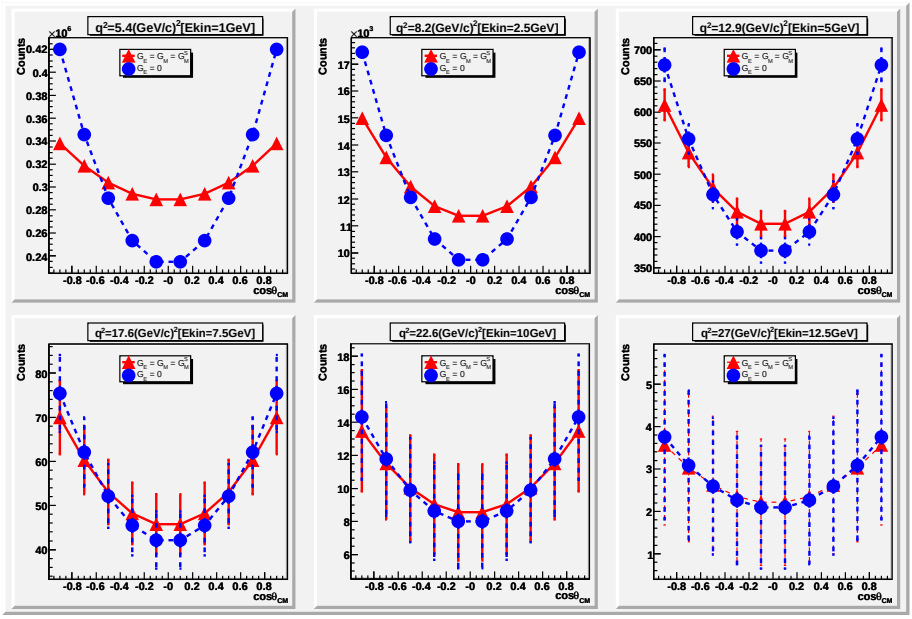

FIG. 26: Angular distribution as a function of $\cos\theta_{CM}$ in the hypothesis of G_E=0 (open squares, dashed line) and G_E=G_M (solid circles), for q^2 values ranging from 5.4 to 27 GeV^2. The value for $|G_M|$ is computed from Eq. (5).

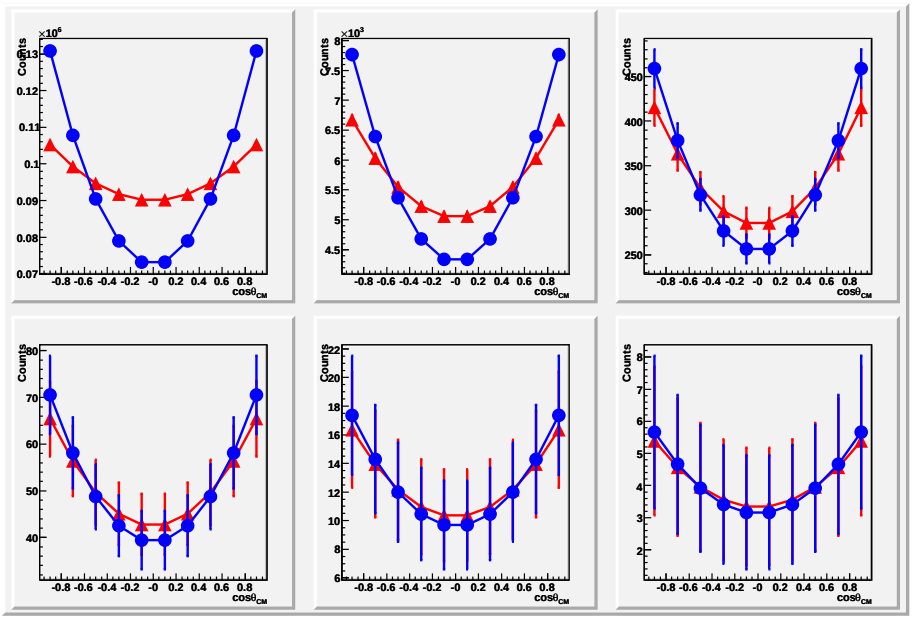

FIG. 27: Same as Fig. 26, for FFs parametrization corresponding to Eq. (6).